PROCEEDINGS OF SPIE

SPIEDigitalLibrary.org/conference-proceedings-of-spie

Time resolved digital holography measurements of the nonlinear optical filters

Balys Momgaudis, Tatiana Amotchkina, Linas Smalakys, Michael Trubetskov, Oleg Pronin, et al.

Balys Momgaudis, Tatiana Amotchkina, Linas Smalakys, Michael Trubetskov, Oleg Pronin, Ferenc Krausz, Vladimir Pervak, Andrius Melninkaitis, "Time resolved digital holography measurements of the nonlinear optical filters," Proc. SPIE 10447, Laser-Induced Damage in Optical Materials 2017, 104470Y (17 November 2017); doi: 10.1117/12.2280538

SPIE.

Event: SPIE Laser Damage, 2017, Boulder, Colorado, United States

Time resolved digital holography measurements of the nonlinear optical filters

Balys Momgaudis[a], Tatiana Amotchkina[b], Linas Smalakys[a], Michael Trubetskov[b], Oleg Pronin[c], Ferenc Krausz[b, c], Vladimir Pervak[c], and Andrius Melninkaitis[a]

[a]Laser Research Center, Vilnius University, Saulėtekio al. 10, 10223 Vilnius, Lithuania
[b]Max-Planck-Institut für Quantenoptik, Hans-Kopfermann-Str. 1, Garching 85748, Germany
[c]Ludwig-Maximilians-Universität München, Am Coulombwall 1, Garching 85748, Germany

ABSTRACT

A special dielectric edge filter extremely sensitive to any change in refractive indices, layer thicknesses and angle of incidence has been investigated using holographic pump-probe measurements at different intensity values. Different physical processes overlapping in time were found to occur, namely the Kerr effect, free-electron generation and their subsequent trapping. A numerical model was used to reproduce the experimental results and decouple these processes.

Keywords: nonlinear coating, edge filter, Kerr effect, nonlinear ionization, time-resolved digital holography, finite-difference time-domain

1. INTRODUCTION

The field of nonlinear optical coatings is gaining moderate interest after promising demonstrations of frequency tripling mirrors,[1] Kerr-sensitive edge filters[2] and other promising applications. However, since these optics operate at high intensity values by design, the topic of laser-induced damage threshold (LIDT) must be addressed. Recent trend in the laser-damage field is to investigate laser-induced damage *in situ* by employing time resolved experimental techniques that provide evidence of nonlinear material response and subsequent dynamical processes.[3–5] Time resolved digital holography (TRDH) pump-probe experiments is a promising technique that provide information about the change in real and imaginary parts of refractive index with both spatial and temporal resolution.[6] However, interpretation of TRDH experiments, especially in stratified media such as multilayer coatings, is a complicated task without appropriate theoretical models that would allow to correctly describe many simultaneous processes that underlie the formation of damage. In this paper we present TRDH measurements of a nonlinear edge filter and an accompanying theoretical model to quantitatively analyze the nonlinear response of the coating.

2. TIME-RESOLVED MEASUREMENTS

Edge filter named F502 was selected for the time-resolved investigation of laser damage. It is comprised of 69 alternating Nb_2O_5 and SiO_2 layers and has steep changes in spectral and angular reflectances (at 1030 nm and 17 deg. respectively). More information about the design, manufacturing and optical characterization of the sample can be found in the paper by Amotchkina *et al.*[2]

Further author information: (Send correspondence to Linas Smalakys)
Linas Smalakys: E-mail: linas.smalakys@ff.vu.lt

Laser-Induced Damage in Optical Materials 2017, edited by Gregory J. Exarhos, Vitaly E. Gruzdev, Joseph A. Menapace, Detlev Ristau, MJ Soileau, Proc. of SPIE Vol. 10447, 104470Y
 · doi: 10.1117/12.2280538

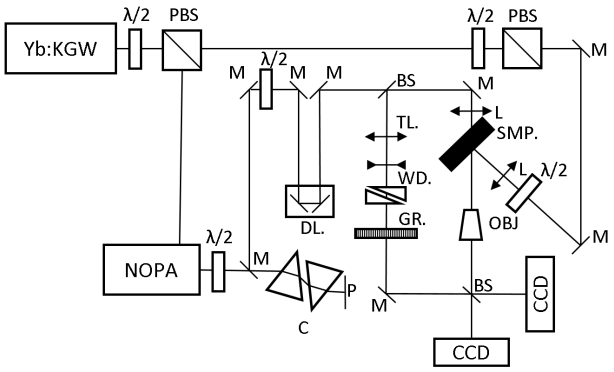

Figure 1. The experimental setup of nonlinear refractive index measurements. PBS - polarizing beam splitter, M - mirrors, BS - neutral beam splitters, P - periscope, C - prism compressor, GR - diffraction grating, WD - glass wedges, OBJ - microscope objective, SMP - sample, TL - telescope, DL - mechanical delay line.

The optical scheme of the experimental time-resolved digital holography setup is shown in Figure 1. An oscillator-amplifier (Yb:KGW) laser system was used to generate 310 fs duration (FWHM) pulses at a central wavelength of 1030 nm. The incoming pulses were split into pump and probe branches by using $\lambda/2$ plate and polarizing beam splitter (PBS). Pump pulses were focused down to a spot of (57.4 $\pm$ 0.6) μm beam diameter ($1/e^2$) on the NMC at 0 degree angle of incidence (s polarization). Fluence level of pump pulses was adjusted by using an attenuator consisting of $\lambda/2$ plate and PBS. Probe pulses were produced by amplifying and compressing spectrally broadened supercontinuum pulses using a noncollinear optical parametric amplifier (NOPA), based on BBO nonlinear crystal pumped by third harmonic of the fundamental pulses.[7] After the amplification and prism-based compression, bandwidth-limited probe pulses with 28 fs duration (FWHM) were produced at central wavelength of 539 nm. After passing through the mechanical delay line, pump pulses were further split into object and reference branches. The object branch contained the investigated NMC sample (placed backwards at 45 degree angle of incidence (p polarization)) and microscope objective. The reference branch contained telescope, fused quartz wedges (to compensate for sample group velocity dispersion) and diffraction grating (to tilt the phase front of the pulses in order expand the spatial interference zone registered on a CCD camera). Object and reference branches were recombined in a modified Mach–Zehnder interferometer. An out of focus interference pattern was registered with the CCD camera. This digital hologram was numerically reconstructed[8] to produce amplitude and phase changes of the probe pulse, caused by the NMC excitations induced by the pump pulse.

The 1-on-1 LIDT of the F502 sample for the conditions of pump pulses was measured prior to the time-resolved experiments. The LIDT value as well as a few intensity values just below and above LIDT (Table 1) were selected for investigation of underlying processes. The excitations were observed in the delay range of up to 2.5 ps after the peak of the pump pulse with a step of 50 fs. Experimental transmittance ratio and phase shift data for all intensity values at selected delays are provided in Figures 2, 3. Negative phase shift due to the nonlinear Kerr effect was apparent at all measured intensity levels. Its temporal shape resembled that of a pump pulse envelope. Generation of free electron gas became evident only at intensities equal to or above LIDT and manifested itself in positive phase shift and reduced transmission of the probe beam around the peak of the pump pulse (the higher the intensity, the earlier the effect starts). At intensities above LIDT, phase flipped back to negative values – a behaviour exhibited in materials with self-trapped excitons.[9]

Table 1. Fluence and intensity levels used for time-resolved investigation of sample F502.

	Pulse energy, μJ	Peak fluence, J/cm^2	Peak intensity, GW/cm^2
80% LIDT	1.58	0.123	395
90% LIDT	1.77	0.137	442
LIDT	1.97	0.152	491
120% LIDT	2.37	0.184	593
145% LIDT	2.83	0.219	707

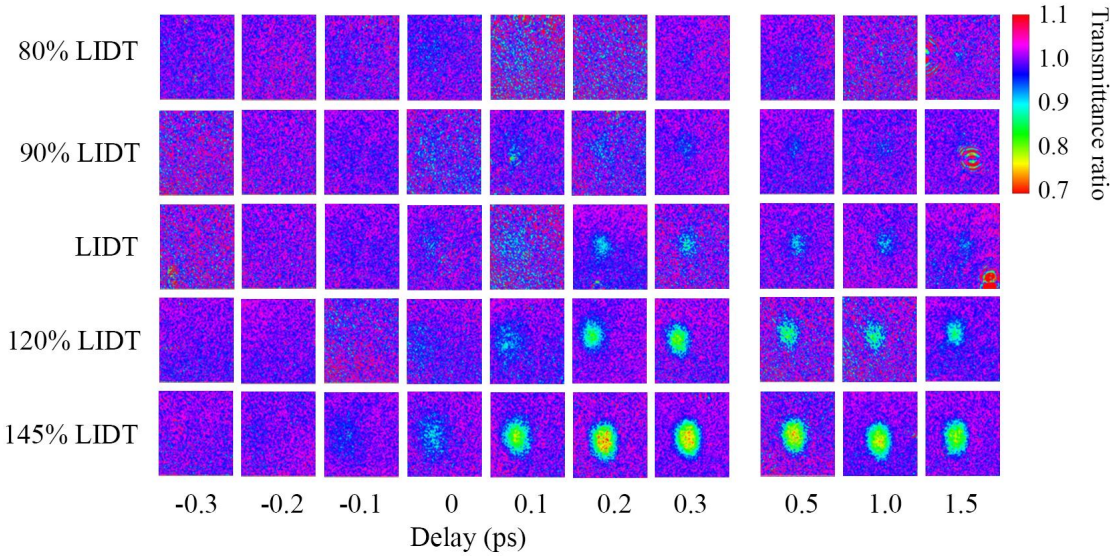

Figure 2. Experimental spatiotemporal transmittance ratio data at different intensity values.

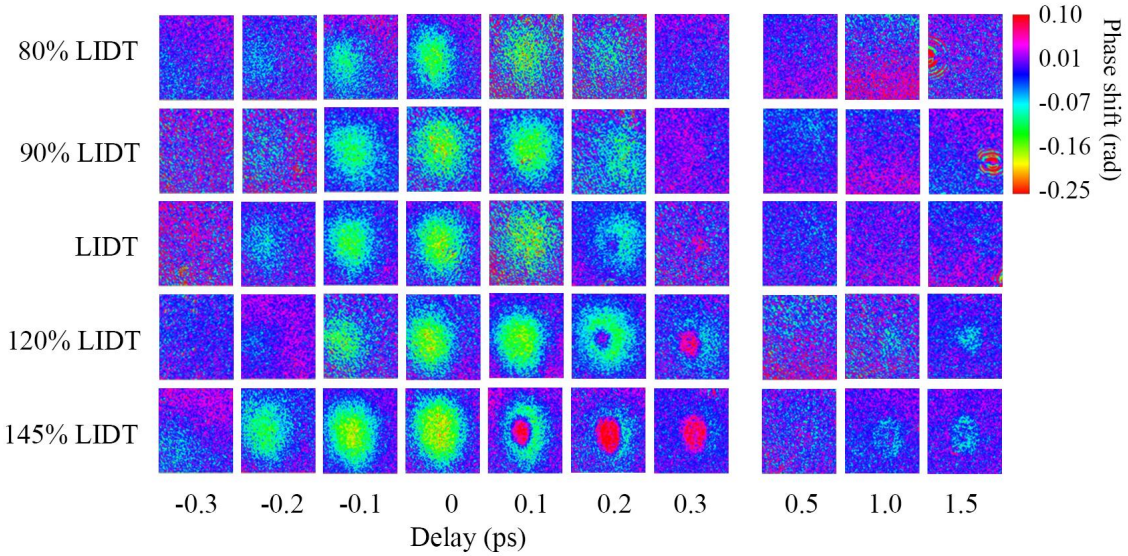

Figure 3. Experimental spatiotemporal phase shift data at different intensity values.

3. THEORETICAL MODEL

Ultrafast response of nonlinear multilayer coating to high intensity femtosecond laser pulses includes multiple ionization and recombination processes making it a highly dynamical system. In order to decouple the processes involved in ultrafast laser damage a theoretical model was developed based on well established techniques: a system of rate equations for free carrier absorption and direct evolution of Maxwell's equations using finite-difference time domain (FDTD) method.

3.1 Material response function

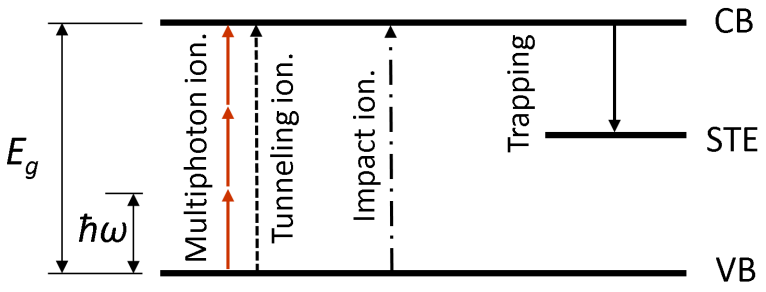

Figure 4. Simplified diagram of energy levels model.

Material's energy band diagram is often simplified and simulated by using coupled rate equations:

$$\frac{\partial N_{CB}}{\partial t} = w_K\left(I\right) + w_{II}\left(I, N_{CB}\right) - w_{CB\to STE}\left(N_{CB}, N_{STE}\right) \tag{1}$$

$$\frac{\partial N_{STE}}{\partial t} = w_{CB\to STE}\left(N_{CB}, N_{STE}\right) \tag{2}$$

w_K – Keldysh ionization rate which includes both multiphoton and tunneling ionizations,[10,11] w_{II} – impact ionization rate and $w_{CB\to STE}$ – trapping rate, which couples self-trapped exciton state to the system:

$$w_{II}\left(I, N_{CB}\right) = \alpha I N_{CB} \tag{3}$$

$$w_{CB\to STE}\left(N_{CB}, N_{STE}\right) = \frac{N_{CB}}{\tau_{CB\to STE}}\left(1 - \frac{N_{STE}}{N_{STE,max}}\right) \tag{4}$$

where N_{STE} is density of self-trapped excitons, $N_{STE,max}$ – maximum density of self-trapped excitons density, $\tau_{CB\to STE}$ – trapping time and N_{CB} density of conduction band electrons. Relaxation to valence band and ionization of trapped states is omitted, because these processes take place on a longer time scale, but can easily be incorporated if multiple pulse regime is of interest. The full graphical representation of the simulated energy band system is shown in Figure 4.

The material model is described through the polarization vector. In our case, the polarization is affected by Kerr effect, conduction band electrons and self-trapped exciton state:

$$\mathbf{P} = \mathbf{P}_{\mathrm{K}} + \mathbf{P}_{\mathrm{CB}} + \mathbf{P}_{\mathrm{STE}} \tag{5}$$

The response of conduction band electrons is taken into account by using the Drude model for free electrons[12] with $\omega_{p,CB}$ as plasma frequency:

$$\mathbf{P}_{\mathrm{CB}} = -\epsilon_0 \frac{\omega_{p,CB}^2}{\left(\omega^2 + \frac{i\omega}{\tau_{CB}}\right)} \mathbf{E} \tag{6}$$

$$\omega_{p,CB} = \sqrt{\frac{N_{CB} e^2}{\epsilon_0 m_{CB}}} \tag{7}$$

The response of self-trapped exciton states is taken into account by assuming the Lorentz model for bound states[12] with $\omega_{p,STE}$ as resonance frequency:

$$\mathbf{P}_{\mathrm{STE}} = \epsilon_0 \frac{\omega_{p,STE}^2}{\left(\omega_{STE}^2 - \omega^2 - \frac{i\omega}{\tau_{STE}}\right)} \mathbf{E} \tag{8}$$

$$\omega_{p,STE} = \sqrt{\frac{N_{STE} e^2}{\epsilon_0 m_{STE}}} \tag{9}$$

m_{CB} is effective mass of conduction band electrons, m_{STE} – effective mass of self-trapped excitons, e – elementary charge, ϵ_0 – vacuum permittivity.

Electric displacement vector $\mathbf{D}$ and complex relative permittivity ϵ_r can then be expressed as:

$$\begin{aligned} \mathbf{D} &= \epsilon_0 \epsilon_r^{(1)} \mathbf{E} + \mathbf{P}_{\mathrm{K}} + \mathbf{P}_{\mathrm{CB}} + \mathbf{P}_{\mathrm{STE}} \\ &= \epsilon_0 \left(\epsilon_r^{(1)} + \chi^{(3)} |\mathbf{E}|^2 - \frac{\omega_{p,CB}^2}{\omega^2 + \frac{i\omega}{\tau_{CB}}} + \frac{\omega_{p,STE}^2}{\omega_{STE}^2 - \omega^2 - \frac{i\omega}{\tau_{STE}}} \right) \mathbf{E} \\ &= \epsilon_0 \epsilon_r \mathbf{E} \end{aligned} \tag{10}$$

$$\epsilon_r = \epsilon_r^{(1)} + \chi^{(3)} |\mathbf{E}|^2 - \frac{\omega_{p,CB}^2}{\omega^2 + \frac{i\omega}{\tau_{CB}}} + \frac{\omega_{p,STE}^2}{\omega_{STE}^2 - \omega^2 - \frac{i\omega}{\tau_{STE}}} \tag{11}$$

The real part of complex dielectric permittivity can be directly used in the FDTD scheme with real fields:

$$\mathrm{Re}\left(\epsilon_r\right) = \epsilon_r^{(1)} + \chi^{(3)} |\mathbf{E}|^2 - \frac{\omega_p^2 \tau_{CB}^2}{1 + \omega^2 \tau_{CB}^2} + \frac{\omega_{p,STE}^2 \left(\omega_{STE}^2 - \omega^2\right)}{\left(\omega_{STE}^2 - \omega^2\right)^2 + \left(\frac{\omega}{\tau_{STE}}\right)^2} \tag{12}$$

However, the inclusion of imaginary part of complex relative permittivity (and thus absorption) is not as straightforward. In order to use it with real fields in the FDTD scheme, we must express it through the conductivity term:[12]

$$\epsilon_r = \mathrm{Re}\left(\epsilon_r\right) + i\mathrm{Im}\left(\epsilon_r\right) = \mathrm{Re}\left(\epsilon_r\right) + i\frac{\sigma}{\epsilon_0 \omega} \tag{13}$$

$$\sigma = \epsilon_0 \omega \mathrm{Im}\left(\epsilon_r\right) \tag{14}$$

where the imaginary part of complex relative permittivity is:

$$\mathrm{Im}\left(\epsilon_r\right) = \frac{\omega_p^2 \tau_{CB}}{\omega\left(1 + \omega^2 \tau_{CB}^2\right)} + \frac{\omega_{p,STE}^2 \frac{\omega}{\tau_{STE}}}{\left(\omega_{STE}^2 - \omega^2\right)^2 + \left(\frac{\omega}{\tau_{STE}}\right)^2} \tag{15}$$

The derived conductivity term (14) only includes absorption by conduction band electrons and self-trapped excitons. An additional absorption term is needed to include Keldysh ionization. This can be accomplished by first equating the loss of laser energy $J_K E$ (where J_K is current density) to energy required to ionize electrons through the Keldysh mechanism $E_{gap} w_K$:[13,14]

$$J_K E = \sigma_K E^2 = E_{gap} w_K \tag{16}$$

The nonlinear conductivity term that accounts for Keldysh ionization σ_K and effective conductivity σ_{eff} of the whole system can then be expressed as:

$$\sigma_K = \frac{E_{gap} w_K}{E^2} \tag{17}$$

$$\sigma_{eff} = \sigma + \sigma_K \tag{18}$$

3.2 Electromagnetic field in layered structures

In order to simulate the propagation of femtosecond laser pulse in layered dynamical system the most fundamental method of solving Maxwell's equations was chosen. The electromagnetic field simulation is based on Maxwell's curl equations.[15] In the one dimensional case (assuming propagation along the z axis) these equations can be written as:

$$\frac{\partial H_y}{\partial z} = \epsilon \frac{\partial E_x}{\partial t} + \sigma E_x \tag{19}$$

$$\frac{\partial E_x}{\partial z} = \mu \frac{\partial H_y}{\partial t} \tag{20}$$

where E_x denotes electric field, H_y – magnetizing field, ϵ – permittivity, σ – conductivity, μ – permeability

The finite-difference time-domain method can be used to discretize these equations using Yee's method,[16] which separates E_x and H_y both in time and space in order to achieve second-order accuracy:[15]

$$E_x^{q+1}[m] = \frac{1 - \frac{\sigma \Delta_t}{2\epsilon}}{1 + \frac{\sigma \Delta_t}{2\epsilon}} E_x^q[m] + \frac{\frac{\Delta_t}{\epsilon \Delta_z}}{1 + \frac{\sigma \Delta_t}{2\epsilon}} \left(H_y^{q+\frac{1}{2}}\left[m + \frac{1}{2}\right] - H_y^{q+\frac{1}{2}}\left[m - \frac{1}{2}\right] \right) \tag{21}$$

$$H_y^{q+\frac{1}{2}}\left[m + \frac{1}{2}\right] = H_y^{q-\frac{1}{2}}\left[m + \frac{1}{2}\right] + \frac{\Delta_t}{\mu \Delta_z} \left(E_x^q[m+1] - E_x^q[m] \right) \tag{22}$$

Δ_z is spatial step, Δ_t – temporal step, m – spatial step index, q – temporal step index. Permittivity ϵ is calculated using the real part of previously derived relative permittivity (12) and effective conductivity from (18) is used as σ. At every temporal time step, ϵ and σ are adjusted by calculating the densities of conduction band electrons and self-trapped excitons using rate equations (1) and (2).

Since the pump pulse is more than 10 times longer than the probe pulse, semi-analytical methods can be used to evaluate relative transmission and phase shift of the probe beam. Transmission can be evaluated by using S-matrix method by taking FDTD grid of complex refractive indices as an input.[17] Transmittance ratio can then be evaluated by comparing transmittance with the linear case. Phase shift can be evaluated directly from B-integral:[18]

$$\delta\phi = \frac{2\pi}{\lambda} \int_{z_1}^{z_2} \delta n(z) dz \tag{23}$$

4. ANALYSIS

In order to perform a quantitative analysis of the 2D time-resolved experimental data (Figures 2, 3), transmittance ratio and phase shift values in the center region of 20x20 pixels were averaged to produce 1D time-resolved data (Figure 5) for the region of highest intensity. A spatial step $\Delta_z = 10$ nm was chosen for the FDTD simulation based on convergence measurements, which resulted in a temporal step of $\Delta_t = 33$ as for the Courant factor of 1.[15]

4.1 Fitting of 1D time-resolved data

All of the one-dimensional curves (transmittance ratio and phase shift at different intensities) were collectively fitted (SLSQP optimization[19]) using the theoretical model described in the previous section. The collective fit was performed instead of many separate fits in order to constrain the model as much as possible. Since the nonlinear response of the coating is dominated by Nb_2O_5 layers (Kerr effect is 10 times stronger[2] and nonlinear ionization is at least 10^{11} times higher in Nb_2O_5 than in SiO_2) only this material's parameters were varied during the fitting procedure. Fitted values of the model's parameters are provided in Table 2 and corresponding transmission ratio and phase shift curves are shown as solid curves in Figure 5.

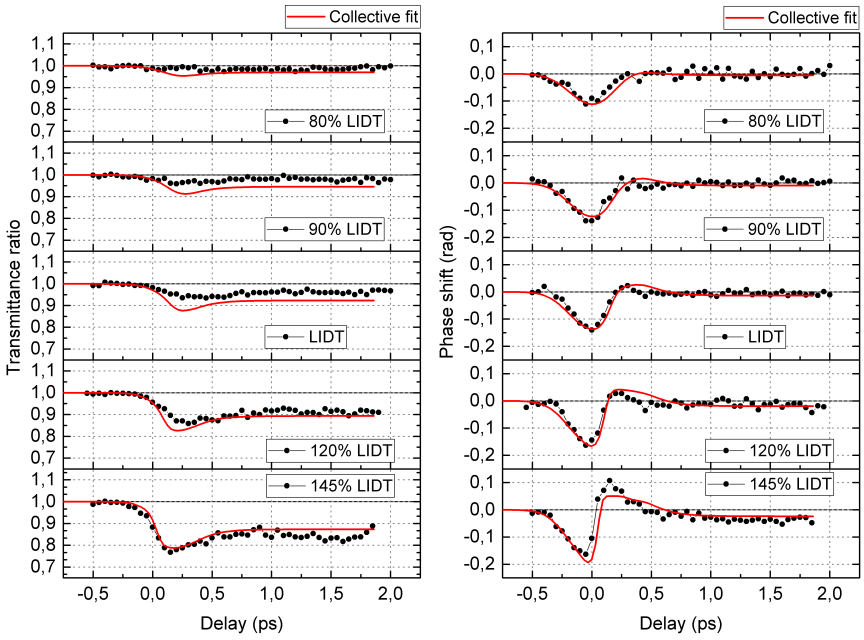

Figure 5. Experimental transmittance ratio and phase shift results. Solid red curves represent the collective fit.

Table 2. Fitted model's material parameters for Nb_2O_5 layers.

Variable	Symbol	Value	Unit
Effective mass of conduction band electrons	m_{CB}	$1.0 \cdot m_e$	kg
Scattering time of conduction band electrons	τ_{CB}	4.1	fs
Coefficient of impact ionization	α	0.0003	m^2/Ws
Effective mass of self-trapped excitons	m_{STE}	$3.3 \cdot m_e$	kg
Scattering time of self-trapped excitons	τ_{STE}	0.1	fs
Trapping time of self-trapped excitons	$\tau_{CB \to STE}$	150	fs
Energy level of self-trapped excitons	E_{STE}	2.9	eV

As can be seen in Figure 5, fitted model is in good agreement with experimental data: it accurately describes both transmittance ratio and phase shift changes for all measured intensity levels. Model predicts 150 fs trapping time for self-trapped excitons which is in good agreement with the same parameter measured for SiO_2.[20]

4.2 Contribution of each layer

Since the model has spatial resolution perpendicularly to the coating, information about the contribution of each Nb_2O_5 layer can also be extracted. Evolution of conduction band electrons and self-trapped excitons for 145% LIDT intensity level is provided in Figure 6 with a corresponding material response in Figure 7 for the top 2 μm of the coating. It can clearly be seen that the majority of nonlinear ionization takes place in only second and third Nb_2O_5 layers, while the contribution from the Kerr effect is more evenly spread out (Figure 7 (a)). The generation of electron plasma begins at the peak of the pulse (Figure 6 (a)), however, electrons are quickly trapped and at the end of the laser pulse only the self-trapped excitons remain (Figure 6 (b)) which are responsible for the absorbtion within the coating (Figure 7 (b)).

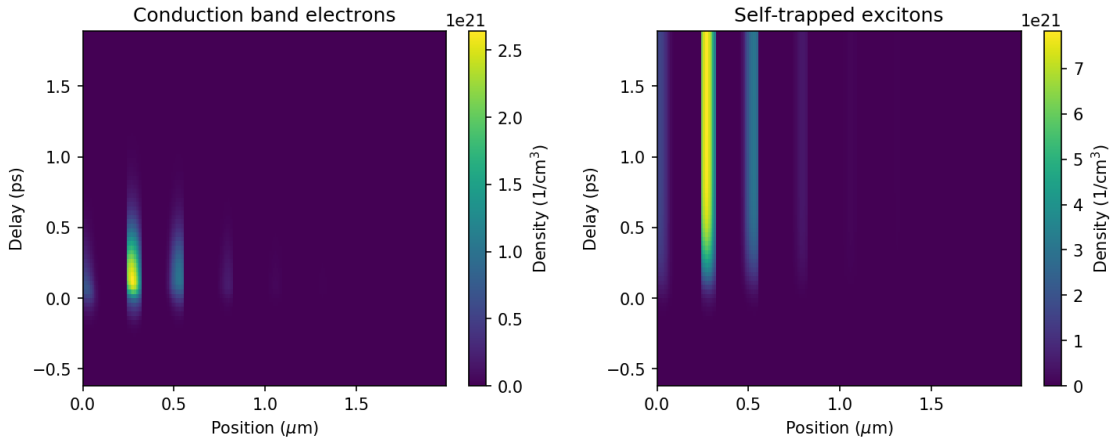

(a) (b)

Figure 6. Evolution of conduction band electrons (a) and self-trapped excitons (b) densities during the 145% LIDT pulse in the first 2 μm of the coating.

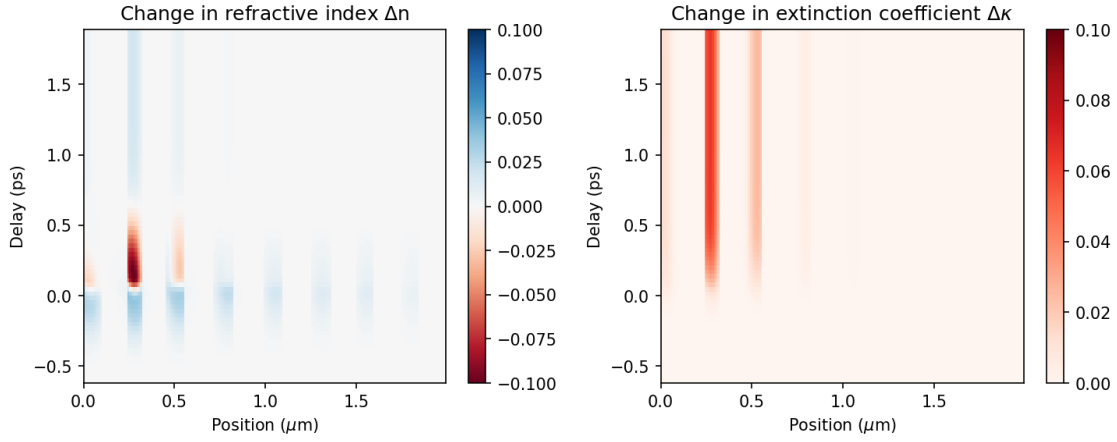

(a) (b)

Figure 7. Evolution of real (a) and imaginary (b) parts of complex refractive index during the 145% LIDT pulse in the first 2 μm of the coating.

4.3 Simulation of time-resolved reflectance

Fitting procedure provided valuable information about the Nb_2O_5 coating which can be used for future investigations of such nonlinear coatings. For example, lets assume a 1030 nm, 300 fs laser pulse is used to exponate the F502 coating at 145% LIDT intensity (0 degree angle of incidence). Our model can be used to evaluate the nonlinear evolution of both angular and spectral reflectance during the laser pulse (Figure 8). We see that nonlinear reflectance is highly dynamical for intensity values higher than LIDT, however, any further analysis of such behaviour is outside the scope of this paper and is left for future work.

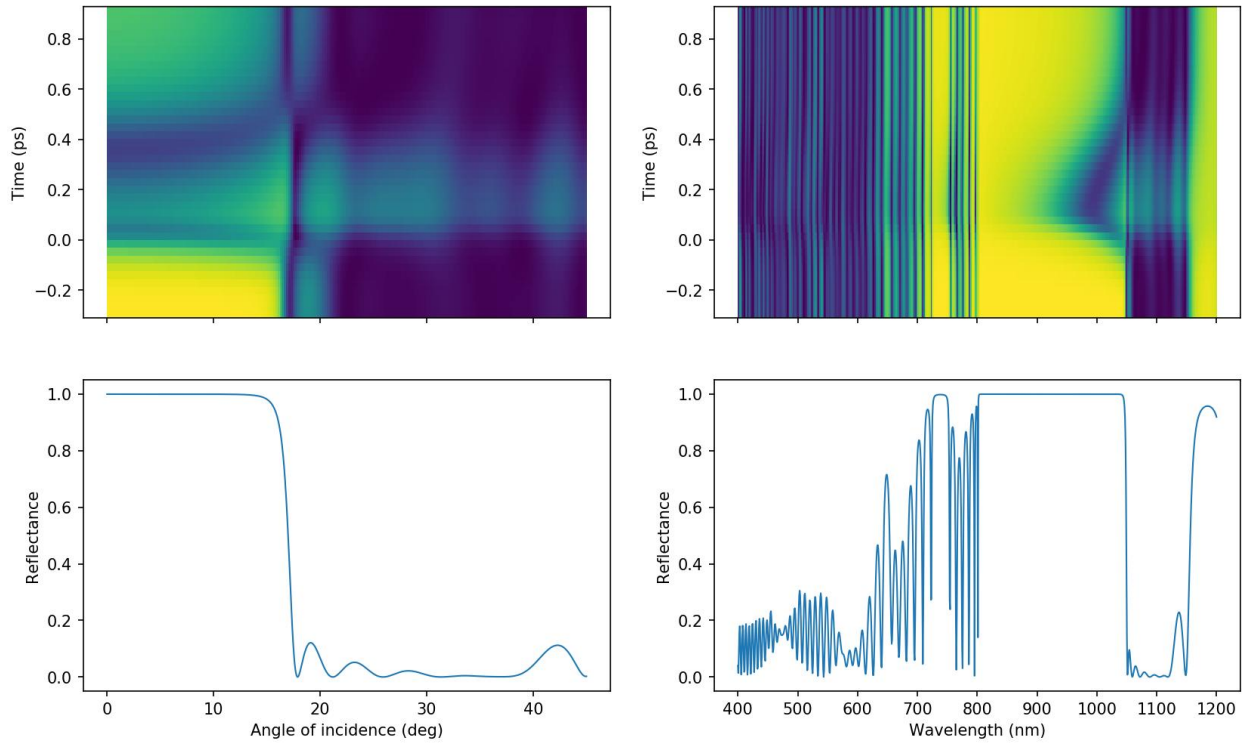

(a) (b)

Figure 8. Evolution of angular (a) and spectral (b) reflectance during the 145% LIDT pulse. Bottom figures show the linear case for respective nonlinear cases.

5. CONCLUSIONS

We performed a series of pump-probe experiments with spatio-temporal and phase-amplitude resolution on multilayer Nb_2O_5/SiO_2 edge filter F502. A one dimensional model was suggested which was found to be in good agreement with both transmittance ratio and phase shift experimental data for all measured intensities. A simple material model based on Keldysh, Drude and Lorentz models seems to be enough to describe nonlinear processess that take place on a time scale of a few picoseconds. Nb_2O_5 was shown to experience trapping of electrons with a time scale very similar to a widely reported temporal constant of 150 fs for SiO_2. Nb_2O_5/SiO_2 coating's nonlinear response is dominated by Nb_2O_5 layers with only a few of the top layers contributing to the nonlinear response. Our model allowed identifying each layer's individual contribution and predicting nonlinear evolution of angular and spectral reflectance.

6. ACKNOWLEDGEMENTS

This work was partially supported by the DFG Cluster of Excellence, "Munich Centre for Advanced Photonics," (http://www.munich-photonics.de). T. Amotchkina has received funding from the European Union's Horizon 2020 research and innovation programme under the Marie Skłodowska-Curie agreement No 657596.

REFERENCES

[1] Rodríguez, C., Günster, S., Ristau, D., and Rudolph, W., "Frequency tripling mirror," *Opt. Express* **23**, 31594–31601 (Nov 2015).

[2] Amotchkina, T., Trubetskov, M., and Pervak, V., "Experimental and numerical study of the nonlinear response of optical multilayers," *Opt. Express* **25**, 12675–12688 (May 2017).

[3] Melninkaitis, A., Šiaulys, N., Smalakys, L., Momgaudis, B., Vaicenavičius, J., Barkauskaitė, S., Sirutkaitis, V., Gallais, L., and Guizard, S., "What time-resolved measurements tell us about femtosecond laser damage?," *Proc. SPIE* **9632**, 96320O–96320O–12 (2015).

[4] Mouskeftaras, A., Guizard, S., Fedorov, N., and Klimentov, S., "Mechanisms of femtosecond laser ablation of dielectrics revealed by double pump–probe experiment," *Applied Physics A* **110**(3), 709–715 (2013).

[5] Mao, S. S., Quéré, F., Guizard, S., Mao, X., Russo, R. E., Petite, G., and Martin, P., "Dynamics of femtosecond laser interactions with dielectrics," *Applied Physics A: Materials Science and Processing* **79**, 1695–1709 (2004).

[6] Šiaulys, N., Gallais, L., and Melninkaitis, A., "Direct holographic imaging of ultrafast laser damage process in thin films.," *Optics letters* **39**(7), 2164–7 (2014).

[7] Kumar, S. K. K., Goswami, T., Bhattacharyya, I., and Goswami, D., "Visible 20-femtosecond pulse generation by double-pass non-collinear optical parametric amplifier," *Current Science* **96**(11), 1496–1500 (2009).

[8] Kim, M. K., [*Principles and techniques of digital holographic microscopy*], Springer, New York, USA (2011).

[9] Guizard, S., Martin, P., Petite, G., D'Oliveira, P., and Meynadier, P., "Time-resolved study of laser-induced colour centres in SiO_2," *Journal of Physics: Condensed Matter* **8**(9), 1281 (1996).

[10] Keldysh, L. V., "Ionization in the field of a strong electromagnetic wave," *Journal of Experimental and Theoretical Physics* **20**(5), 1307–1314 (1965).

[11] Jupé, M., Jensen, L., Melninkaitis, A., Sirutkaitis, V., and Ristau, D., "Calculations and experimental demonstration of multi-photon absorption governing fs laser-induced damage in titania," *Opt. Express* **17**, 12269–12278 (Jul 2009).

[12] Fox, M., [*Optical Properties of Solids*], Oxford University Press, New York, USA, 2nd ed. (2010).

[13] Peñano, J. R., Sprangle, P., Hafizi, B., Manheimer, W., and Zigler, A., "Transmission of intense femtosecond laser pulses into dielectrics," *Phys. Rev. E* **72**, 036412 (Sep 2005).

[14] Buschlinger, R., Nolte, S., and Peschel, U., "Self-organized pattern formation in laser-induced multiphoton ionization," *Phys. Rev. B* **89**, 184306 (May 2014).

[15] Taflove, A., [*Computational Electrodynamics: The Finite-Difference Time-Domain Methods*], Artech House, Norwood, USA (1995).

[16] Yee, K., "Numerical solution of initial boundary value problems involving Maxwell's equations in isotropic media," *Antennas and Propagation, IEEE Transactions on* **14**, 302–307 (May 1966).

[17] Yuffa, A. and Scales, J., "Object-oriented electrodynamic S-matrix code with modern applications," *Journal of Computational Physics* **231**, 4823–4835 (2012).

[18] Boyd, R. W., [*Nonlinear Optics*], Academic Press, Waltham, USA, 3rd ed. (2008).

[19] Kraft, D., [*A software package for sequential quadratic programming*], Deutsche Forschungs- und Versuchsanstalt für Luft- und Raumfahrt Köln: Forschungsbericht, Wiss. Berichtswesen d. DFVLR (1988).

[20] Guizard, S., Martin, P., Daguzan, P., Petite, G., Audebert, P., Geindre, J. P., Santos, A. D., and Antonnetti, A., "Contrasted behaviour of an electron gas in MgO, Al2O3 and SiO2," *EPL (Europhysics Letters)* **29**(5), 401 (1995).